

QGP flow fluctuations and the characteristics of higher moments

D. J. Wang^{1,2}, L. P. Csernai¹, D. Strottman¹, Cs. Anderlik³, Y. Cheng²,
D. M. Zhou², Y. L. Yan⁴, X. Cai² and B. H. Sa⁴,

¹ *Department of Physics and Technology, University of Bergen, 5007 Bergen, Norway*

² *Institute of Particle Physics, Huazhong Normal University, 430079 Wuhan, China*

³ *Uni Computing, Thormøhlensgate 55, N-5008 Bergen, Norway*

⁴ *China Institute of Atomic Energy, P. O. Box 275 (10), 102413 Beijing, China*

(Dated: November 9, 2018)

The dynamical development of expanding Quark-gluon Plasma (QGP) flow is studied in a 3+1D fluid dynamical model with a globally symmetric, initial condition. We minimize fluctuations arising from complex dynamical processes at finite impact parameters and from fluctuating random initial conditions to have a conservative fluid dynamical background estimate for the statistical distributions of the thermodynamical parameters. We also avoid a phase transition in the equation of state, and we let the matter supercool during the expansion. Then central Pb+Pb collisions at $\sqrt{s_{NN}} = 2.76$ TeV are studied in an almost perfect fluid dynamical model, with azimuthally symmetric initial state generated in a dynamical flux-tube model. The general development of thermodynamical extensives are also shown for lower energies. We observe considerable deviations from a thermal equilibrium source, changing skewness and kurtosis by time depending on beam energy as a consequence of the fluid dynamical expansion arising from a least fluctuating initial state.

PACS numbers: 12.38.Mh, 25.75.-q, 25.75.Nq, 51.20.+d

I. COLLECTIVE FLOW OF GLOBAL SYMMETRY

In heavy ion collisions collective flow has been measured and azimuthal asymmetry was determined from v_1 to v_8 . At the highest energies in central collisions fluctuations dominate arising from fluctuating initial configurations, and the most dominant flow harmonic is v_3 . These are collective flow fluctuations and have no direct connection to the fluctuations arising from a phase transition in the Equation of State (EoS) [1–4].

The fluctuations arising from the pure fluid dynamics without hadronization are studied in this work. We present a set of calculations, what kind of effects a possibly most conservative relativistic fluid dynamical model exhibits in higher moments of statistical parameters for extensive densities, as skewness and kurtosis, without including any effect associated with a phases transition, in the EoS, in the transport properties, or in special thermodynamical phase space trajectories [5–7], or in special freeze out mechanisms. This study complements a large number of studies with the opposite goal, aiming to analyze the consequences of the above mentioned effects. Contrary to the effort to eliminate all these effects, we still obtain energy dependent changes in the skewness and kurtosis.

We use an EoS without a phase transition and include the possibility of supercooling: we choose the MIT Bag model with parameters fixed to the initial values (two flavors and massless quarks and gluons, and the bag constant is $B = 0.397$ GeV/ fm^3). In addition to omitting the freeze out and its effects, we also avoid to take into account viscosity (except the unavoidable numerical viscosity), thus also the temperature dependence of viscosity near the critical point [8], which may lead to additional

changes of the critical fluctuations in a viscous fluid dynamical evolution.

In peripheral collisions, on the other hand, the initial asymmetry is dominated by the almond shape of the participant matter. This results in a strong elliptic flow, while the directed flow measured in the ALICE TPC appeared to be weak and dominated by random fluctuations.

Computational Fluid Dynamics (CFD) predictions indicated a new directed flow structure: due to the large angular momentum of the initial state in peripheral collisions the anti-flow peak observed at high SPS and RHIC energies is rotating forward, and at sufficiently high beam energy, $v_1(y)$ will start to peak at positive rapidities, i.e. on the same side where the projectile spectator residues arrive after the collision [9]. This happens because the initial angular momentum leads to a faster rotating initial system, and this rotation moves the dominant directed flow peak forward before the expansion from the pressure would slow down the rotation. The observation of this peak is not easy because of the beam directed fluctuations of the initial state.

At high energies the dimensionless shear viscosity over the entropy density, η/s , of the QGP is becoming small [10], and η/s as a function of temperature has a minimum at the critical temperature [11]. So the Reynolds number may exceed one, and turbulent phenomena may start to occur. On the other hand, η/s at a critical point does not necessarily have a minimum, since the dynamical universality class of a possible critical point of QCD is the H-model in Hohenberg and Halperin's classification [12, 13], the shear viscosity may diverge at a possible QCD critical point. This would damp instabilities.

Recently in the same CFD model with the Particle in Cell (PIC) method, it was observed that in peripheral col-

lisions with low viscosity (and low numerical viscosity) a Kelvin-Helmholtz (KH) instability starts to develop [14], which enhances the rotation effect and the spatial variance of the flow pattern. The flow effects depend on the initial state profile and on the viscosity. Turbulence appears only for small viscosity, which indicates the critical point of the matter [11], and it is a sensitive measure of viscosity and its minimum at the critical point.

Our CFD simulations of the LHC heavy ion collisions suggest that collective directed $v_1(y)$ flow function can be measured if the Globally asymmetric flow component and the random flow arising from the initial state y_{CM} -fluctuations can be separated. In hydrodynamical calculations we see that the v_1 Global flow can change the peak position to "forward" with increasing beam energy and initial angular momentum. This is a result of our tilted initial state with shear flow [15, 16], in which the angular momentum from the increasing beam momentum may supersede the expansion driven by the pressure.

The above described phenomena contribute to an increased spatial spread of the matter during the collision. These effects are present even if we do not have a phase transition in our EoS [17]. Our present goal is to determine the lowest possible deviation from an ideal thermal source in a least fluctuating CFD evolution. Thus, we eliminate random initial state fluctuations and all azimuthal asymmetries in a head-on collisions to obtain a most symmetric distribution, and study the spatial fluctuation of thermodynamical quantities in such a system. This then can be compared to the effects caused by the phase transition [1–3, 5–7, 18–20].

Most random fluctuations lead to close to Gaussian distribution, nevertheless the dominant fluid dynamical expansion, even if all special sources are eliminated or minimized may lead to more complex non-gaussian fluctuations and higher statistical moments.

For a realistic reaction model we have to describe the final stage of the reaction also. We have a Multi Module Model approach to describe high energy heavy ion collisions in the RHIC and LHC energy range. Then from the locally equilibrated QGP we have to form hadrons. We do not assume that the hadronization happens in chemical equilibrium as this would take too long time [21, 22] and would not allow for baryons of high strangeness. Thus we use the simplest bag model approach, which in the pure QGP domain, yields similar results to more detailed parametrizations fitted to lattice predictions [23].

In order to be able to hadronize rapidly we have to assume a fast, non-equilibrium hadronization and freeze out with either a Cooper-Frye based method with a local sudden change or a sudden transition to a parton and hadron cascade model, e.g. [24], which can describe rapid hadronization without the assumption of chemical equilibration. This final stage should additionally increase the deviations from the local statistical equilibrium. Thus, the final observed (or calculated) particle distribution, which contains already the influence of the

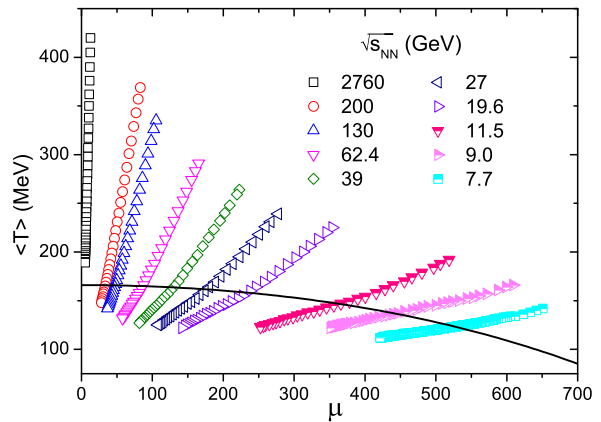


FIG. 1. (color online) The trajectory of fluid dynamical development of QGP fluid at different beam energies as indicated in the figure. Open squares belong to central Pb+Pb collisions, the others are central Au+Au collisions, these are calculated at a cell size resolution of $dx = dy = dz = 0.575$ fm, and time step $\Delta t = 0.04233$ fm/c. The hadronic freeze out curve [25] is indicated by a full black line. The CFD evolution is calculated well beyond this curve. This is possible as the CFD model can describe supercooled QGP fluid also. The viscosity is minimal and only the numerical viscosity is considered in the calculations. These can be performed down to FAIR and NICA energies, although the use of supercooled QGP EoS has constrained validity at these low energies.

rapid hadronization and freeze out, should be compared to the basic fluctuations arising from a (least fluctuating) CFD distribution estimate.

It is also important to mention that different thermodynamical parameters (especially intensives and extensives) do not have to show the same critical fluctuation properties, so we have to study the fluctuations of several parameters. Furthermore the statistical physics estimates assume a single thermal source at or near the critical point, while we estimate here also the effects of spatial fluctuations, which arise from a dynamically expanding fluid flow even in the least fluctuating configuration.

II. FLOW DEVELOPMENT

The dynamically developing flow pattern leads to a spatial distribution of all thermodynamical quantities, while the system expands rapidly. We assume that the most probable scenario is a pre-equilibrium development described by linear flux-tube expansion independently at each point of the transverse, $[x, y]$, plane until local equilibrium is reached at a space-time hypersurface. By this time at high energies we reach a (nearly) equilibrated Quark-gluon Plasma (QGP) state, which then expands and supercools. This intermediate stage is described with a CFD model using the PIC method. Finally the supercooled QGP can hadronize rapidly and almost simultaneously it freezes out. This final stage of the reaction can

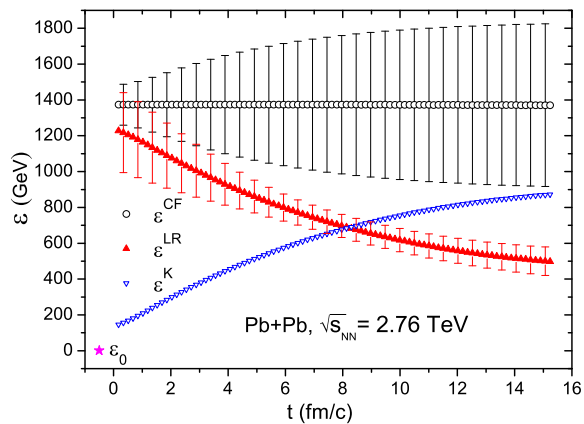


FIG. 2. (color online) The average specific energy density in the calculational frame (ε^{CF}), the average specific internal energy density in the local rest frame (ε^{LR}) and the average specific kinetic energy ($\varepsilon^K = \varepsilon^{CF} - \varepsilon^{LR}$) are calculated by the PIC hydro model in central collisions at $\sqrt{s_{NN}} = 2.76$ TeV. The star indicates $\varepsilon_0 = 0.938$ GeV, the initial specific internal energy before collision. The error bars indicate the variance, σ .

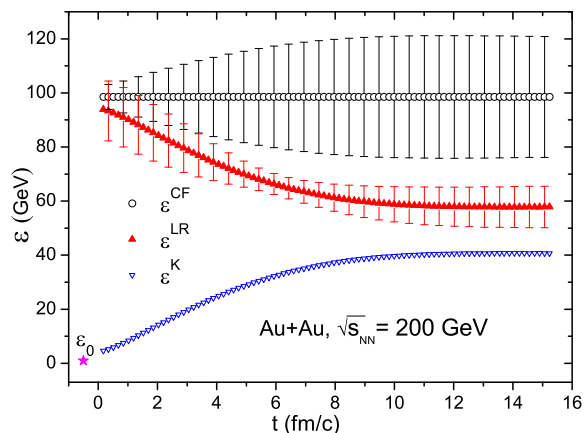


FIG. 3. (color online) The average specific energy density in the calculational frame (ε^{CF}), the average specific internal energy density in the local rest frame (ε^{LR}) and the average specific kinetic energy (ε^K) are calculated by the PIC hydro model in central collisions at $\sqrt{s_{NN}} = 200$ GeV. $\varepsilon_0 = 0.938$ GeV is the initial internal energy before collision. The kinetic energy is the difference between ε^{CF} and ε^{LR} .

be described by a non-equilibrium model.

The CFD model is using N fluid cells, $i = 1, 2, \dots, N$, where with time and expansion the number of fluid cells is increasing. Thus, each cell carries less and less baryon charge with time, and a different amount. Therefore to calculate the volume average and the distribution over the volume we weight the fluid cells by the amount of baryon charge they carry.

Thus the weighted average of a quantity x is defined

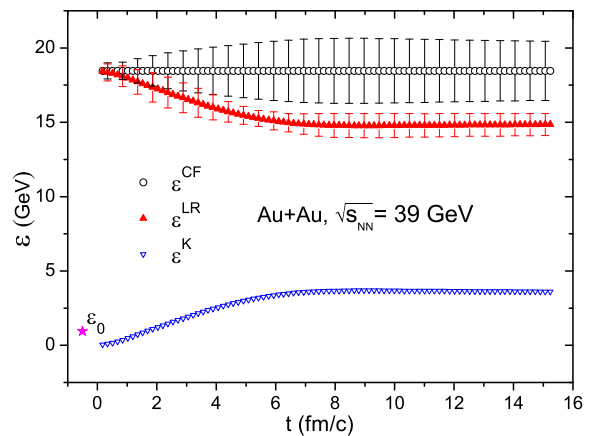


FIG. 4. (color online) The average specific energy density in the calculation frame (ε^{CF}), the average specific internal energy density in the local rest frame (ε^{LR}) and the average specific kinetic energy (ε^K) are calculated by the PIC hydro model in central collisions at $\sqrt{s_{NN}} = 39$ GeV. $\varepsilon_0 = 0.938$ GeV is the initial internal energy before collision. The kinetic energy is the difference between ε^{CF} and ε^{LR} . Observe that at 7 fm/c the specific internal energy and kinetic energy change stalls indicating that the majority of the cells reached zero pressure, the FO boundary. This coincides with the crossing point of the FO curve in Fig. 1, indicating that beyond that point the assumed development in the supercooled QGP is overstretching the applicability of the CFD calculation.

as

$$\langle x \rangle \equiv \sum_i x_i \cdot w_i, \quad \text{where} \quad w_i = \frac{n_i^{CF} \cdot V_i}{N_{tot}}, \quad (1)$$

and V_i is the volume of i^{th} fluid cell, n_i^{CF} is the baryon density in the Calculational Frame (CF), which is the c.m. frame in the present calculations, and $n_i^{CF} = n_i^{LR} \gamma_i$ (where n_i^{LR} is the baryon density in Local Rest Frame), so that $N_{tot} = \sum_i n_i^{LR} \gamma_i V_i$, therefore $\sum_i w_i = 1$.

The CFD stage of this development is shown in Fig. 1, where the time development of the average thermodynamical quantities is shown in the temperature, T and baryon chemical potential, μ , plane and the full black line is the hadronic freeze out curve. In the present work we analyze the CFD stage, and analyze statistically the space-time development of both the intensive and specific extensive thermodynamical variables. We study central collisions only, to avoid the effects from azimuthal flow asymmetries and from particle emission from projectile and target residues (spectator evaporation) [26].

For a variable x the averages and various order moments of cell-by-cell distributions can be written as

$$\langle x^n \rangle = \int x^n P(x) dx = \sum_i x_i^n w_i, \quad (2)$$

$$M^{(n)} = \langle (x - \langle x \rangle)^n \rangle = \int (x - \langle x \rangle)^n P(x) dx$$

$$= \sum_i (x - \langle x \rangle)^n w_i, \quad (3)$$

where $P(x)$ is the spatial distribution weighted by the baryon charge density in the CF. The spatial variance, the skewness and the kurtosis can be obtained from these moments:

$$\sigma^2 = \langle (x - \langle x \rangle)^2 \rangle = M^{(2)}, \quad (4)$$

$$S = \frac{\langle (x - \langle x \rangle)^3 \rangle}{\sigma^3} = \frac{M^{(3)}}{(M^{(2)})^{3/2}}, \quad (5)$$

$$\kappa = \langle \frac{(x - \langle x \rangle)^4}{\sigma^4} \rangle - 3 = \frac{M^{(4)}}{(M^{(2)})^2} - 3. \quad (6)$$

By using this average, first we can calculate specific extensives, which are governed by strict conservation laws. The total baryon charge, energy and momentum conservations are governed by the continuity equation and by the relativistic Euler equation.

$$N^\mu{}_{,\mu} = 0, \quad (7)$$

$$T^{\mu\nu}{}_{,\nu} = 0, \quad (8)$$

and as a consequence, the total momentum in the center of mass (c.m.) frame should remain zero during the development, while the average specific energy per net nucleon number

$$\langle \varepsilon^{CF} \rangle \equiv \frac{T^{00}}{N^0} = const. \quad (9)$$

should remain constant in CF.

In most experiments the observable is the total charged particle multiplicity. This number is proportional to the energy density and not the net baryon charge. That is the reason we study the energy density. The energy is characterized by the "specific energy density", i.e., by the energy per unit net baryon charge. As you can see, the different parts of the energy development undergo significant changes with time, which may contribute to the statistical properties of the produced particles.

The average specific energy density in CF can be expressed as:

$$\langle \varepsilon^{CF} \rangle = \sum_i \frac{e_i^{CF}}{n_i^{CF}} \frac{n_i^{CF} V_i}{N_{tot}} = \sum_i \frac{e_i^{CF} V_i}{N_{tot}}. \quad (10)$$

Similarly we can obtain the average specific energy density in the local rest frame (LR):

$$\langle \varepsilon^{LR} \rangle = \sum_i \frac{e_i^{LR}}{n_i^{LR}} \frac{n_i^{CF} V_i}{N_{tot}} = \sum_i \frac{e_i^{LR} \gamma_i V_i}{N_{tot}}. \quad (11)$$

These quantities are shown in Figs. 2,3,4. Most importantly the average specific energy remains constant during the time development, and its value is the initial beam energy, $\langle \varepsilon^{CF} \rangle = \frac{1}{2} \sqrt{s_{NN}} = 1.38$ TeV. Due to the CFD expansion, the average specific internal energy,

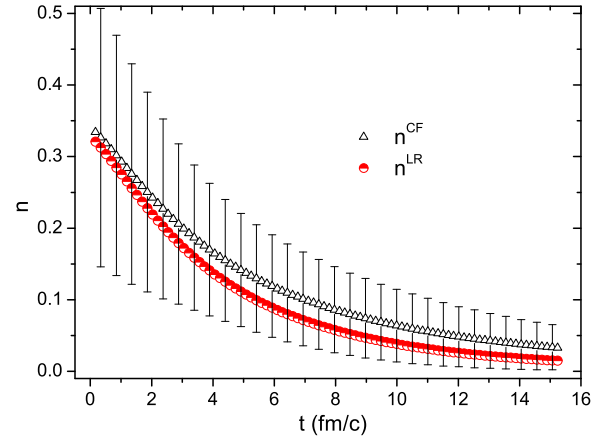


FIG. 5. (color online) The average baryon charge density in the calculation frame (n^{CF}) and in the local rest frame (n^{LR}) calculated by the PIC hydro model in central Pb+Pb collisions at $\sqrt{s_{NN}} = 2.76$ TeV. The error bars indicate the variance, σ , for n^{CF} . The variance is about the same for the invariant specific density, n^{LR} .

$\varepsilon^{LR} = e/n$, decreases as the system expands, while the expansion leads to increased average specific kinetic energy, $\varepsilon^K \equiv \varepsilon^{CF} - \varepsilon^{LR}$. Of course these quantities vary in the space-time during the CFD evolution. Their spatial variances, σ_x , are shown in eq. (4), is also indicated by the error bars in Figs. 2,3,4. Although the average of ε^{CF} remains constant its variance is increasing due to the expansion, which generates increasing number of low density cells. The lower energies give similar results. The three figures demonstrate how much part of the energy is converted into kinetic energy. At the highest energy by the time of 8 fm/c, half of the total available is converted into flow while at lowest shown beam energy, at $\sqrt{s_{NN}} = 39$ GeV, it is only 20%.

Similarly, the net baryon number, $N_{tot} = \sum_i n_i^{LR} \gamma_i V_i$, is exactly conserved in the calculations, as the marker particles carry fixed baryon charge and these are conserved until they are in the calculation grid. At the same time the average baryon charge density is decreasing. We can characterize this by the invariant scalar, LR, baryon density as well as by the CF baryon density. Their averages can be expressed as:

$$\langle n^{CF} \rangle = \sum_i n_i^{CF} \frac{n_i^{CF} V_i}{N_{tot}} = \sum_i (n_i^{CF})^2 \frac{V_i}{N_{tot}}. \quad (12)$$

Similarly we can obtain the average of the invariant scalar baryon density

$$\langle n^{LR} \rangle = \sum_i n_i^{LR} \frac{n_i^{CF} V_i}{N_{tot}} = \sum_i (n_i^{LR})^2 \frac{\gamma_i V_i}{N_{tot}}. \quad (13)$$

The time dependencies of the two densities are shown in Fig. 5. We observe that both densities decrease with time, and the density calculated in CF is larger than the

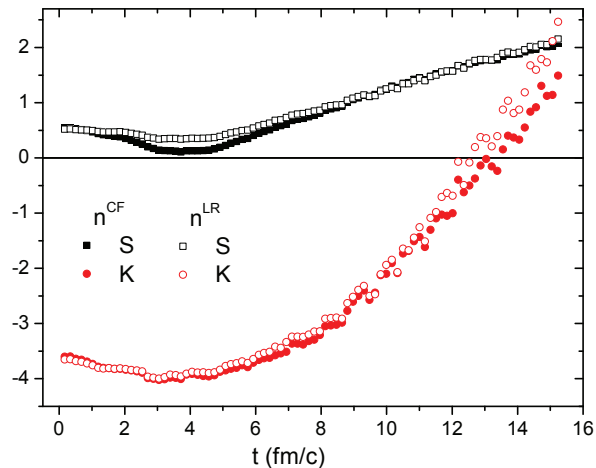


FIG. 6. (color online) The time development of the skewness and kurtosis of the distribution of the net baryon density, n^{CF} , n^{LR} , for central Pb+Pb collision at $\sqrt{s_{NN}} = 2.76$ TeV. The skewness of the baryon charge is positive for both densities indicating an increasingly longer high density tail of the distribution. The kurtosis is initially negative, and turns positive only at very late stages. This is arising from the initial condition where the baryon charge is uniformly distributed in each longitudinal "streak". Around 4 fm/c n^{CF} is visibly smaller than n^{LR} indicating that the apparent density in the CF is more uniform than the invariant scalar density.

density calculated in the LR. Their variance is decreasing with time.

A. Late stages of expansion

As mentioned above the EoS of our perfect fluid dynamical model is ideal QGP, in the form of the MIT Bag model. The parameter of the Bag constant is fixed until the local pressure is positive. In order to be able to calculate the continued expansion in the supercooled QGP we set and fix the pressure to zero and decrease the Bag constant so that the expansion in the supercooled state remains adiabatic [27].

Usually this happens only in very few cells before the estimated average Freeze Out (FO) time (less than 10% of the cells), but we did continue the CFD calculations well into the supercooled state when the zero-pressure cells amounted to 30-40% of the total volume.

In some of the thermodynamical variables this change is exhibited by a change of the development trend line. At the same time the energetic characteristics of the EoS are realistic, so the overall development and the basic quantities are well estimated even during the supercooled stage.

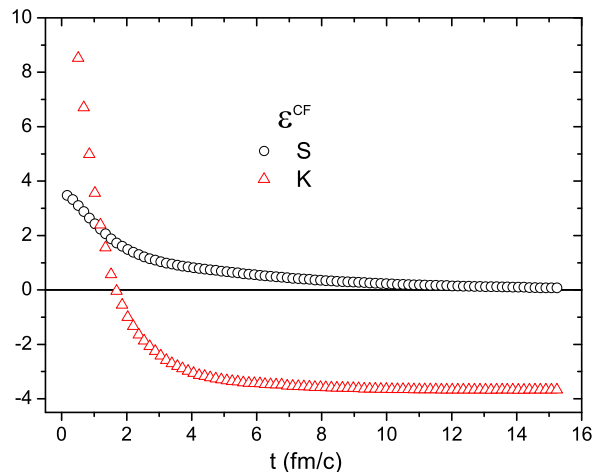


FIG. 7. (color online) The time development of the kurtosis, K , and skewness, S , of the distribution of the specific energy density in the CF, ϵ^{CF} , for central Pb+Pb collisions at $\sqrt{s_{NN}} = 2.76$ TeV. The skewness is positive, decreasing towards zero with time, indicating a longer high energy tail, especially at early stages where we have more cells with high energy QGP, and high kinetic energy as discussed in ref. [19]. The kurtosis is initially positive indicating a high energy density QGP with small spread but decreases with time and it is becoming negative at 2 fm/c. This is caused by populating low energy density supercooled states at later stages.

III. SKEWNESS AND KURTOSIS

In the present work we assume a single QGP phase. We study the features the energy density and net baryon density variations exclusively arising from the fluid dynamics. This dynamical change is not observable directly, only at the freeze out hypersurface which is simultaneous or close to the hadronization. At this point the hadronization may significantly modify the statistical fluctuations [20]. This work evaluates the fluctuations from the previous fluid dynamical evolution. In this part we study the skewness and kurtosis of the specific energy density and the baryon density according to Eq. (5) and Eq. (6). In Fig. 6, we can see that the kurtosis of the baryon density calculated in different frames are similar, the kurtosis is negative at first and then turns to be positive around $t = 13$ fm/c. The skewness is always positive. At $t = 4$ fm/c, both densities have a minimum, but the skewness value in the local rest frame is almost twice larger than in the calculational frame. This indicates that the contribution of the flow makes the distribution close to Gaussian.

In Fig. 7 we can see that the kurtosis of the specific energy in CF, ϵ^{CF} , changes sign from positive to negative, while the skewness is always greater than zero. This is not the same when compared to the results calculated in the local rest frame, which are shown in Fig. 8, where skewness changes sign from negative to positive.

The change of statistics with the changes of the EoS is

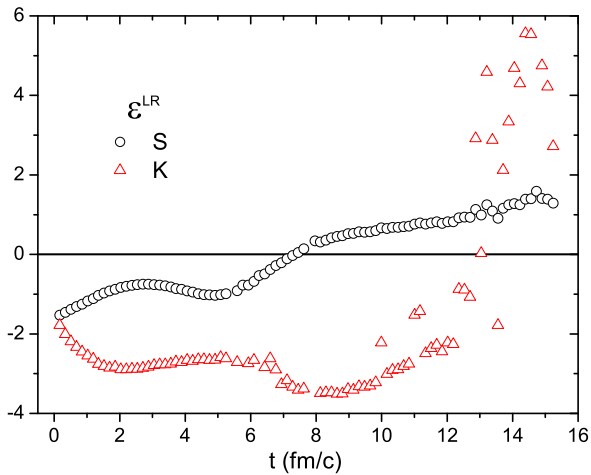


FIG. 8. (color online) The time development of the kurtosis, K , and skewness, S , as in Fig. 7, but for the invariant scalar specific energy density, ε^{LR} , distribution. In case of the invariant scalar specific energy distribution, the skewness changes sign at 7 fm/c. Unlike in Fig. 7 the skewness is initially negative indicating a wider spread in the invariant energy density distribution, which can also be attributed to the presence of QGP.

best seen in Fig. 8 for the invariant specific energy distribution ε^{LR} , although the amplitude of the change is small. The quantity ε^{LR} , does not include the contribution from the kinetic energy, thus it is the best measure of changes in the EoS. The changes are still observable contrary to the fact that the QGP to HM transition is not included in the EoS, but we still have a transition from ideal QGP to the supercooled, zero pressure QGP, where the energy density decreases with the decreasing bag constant.

It is interesting to compare the skewness of the two types of energy densities in Fig. 9, ε^{CF} and ε^{LR} . While ε^{CF} , which contains all kinetic energy, has always a positive skewness, i.e. the distribution is more uniform. The internal energy, ε^{LR} , which increases gradually, has initially negative skewness, meaning a more spread out, fluctuating distribution, which becomes positive later, actually at and after the estimated FO time, when the matter is supercooled and characterized by zero pressure and reduced Bag constant. We can also note that the cross point of the skewness in CF and in LR is around 8 fm/c, which is the same as in Fig. 2, where the trajectories of the Local Rest energy and the Kinetic energy cross. The experimental observations do not show clearly the expected phase transition behavior [20]. That is why we study alternative origins of the fluctuations. The skewness and kurtosis changes are of the same order of magnitude as from critical fluctuations, therefore both effects should be studied.

In a multi-module or hybrid-model construction (e.g where the PIC hydro stage is matched to a parton and

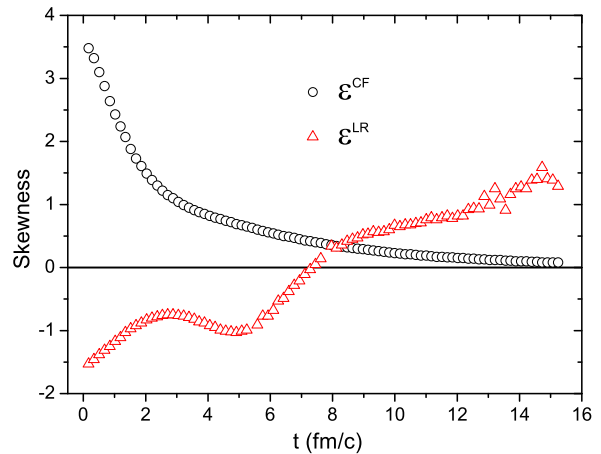


FIG. 9. (color online) The time development of the skewness, K , for the CF specific energy density, ε^{LR} , and the invariant scalar specific energy density, ε^{LR} , distribution. The invariant scalar specific energy distribution changes sign at the typical FO moment, 8 fm/c.

hadron cascade model PACIAE), the flow features are matched [28] to a subsequent dynamical model which describes dynamical, non-equilibrium, rapid hadronization. These types of models can describe realistically the statistical properties and a dynamical phase transition, which provide the hadron distribution in the final stage. This stage would then explicitly describe the random fluctuations arising from the phase transition also.

In ref. [29] a mixed particle method is introduced, which could separate the fluctuations arising from local critical fluctuations. The mixed events are actually eliminating two particle correlations, and only the single particle distributions remain. Thus for central events these are mainly local correlations which may arise from local fluctuations caused by energy and baryon charge clustering in a phase transition. The method separates the consequences of such correlations.

This method can be used both in hybrid model calculations and in experiments, to separate the fluctuation effects from the collective flow and the phase transition dynamics.

IV. CONCLUSIONS

We studied in a fluid dynamical model the time development of spatial distribution averages and variances of thermodynamical variables in high energy heavy ion collisions. We assumed an Equation of State for Quark Gluon Plasma only, but including supercooled QGP also where the pressure is dropped to zero. We studied central collisions, without initial state fluctuations to minimize fluctuations arising from complex anisotropic flow patterns. Including the supercooled QGP we could describe the late stages of the collisions expanding up to

the phase transition boundary [25] and beyond (Fig. 1). In addition to the average temperature and chemical potential we also studied the developments of average energy densities and baryon densities as well as their variances (Figs. 2,3,4,5). The dynamical developments of these variables showed the expected, monotonic dynamical behavior, even beyond the physical FO times, where we overstretched the applicability of the fluid dynamical model.

Our FD model did not include the rapid hadronization and the random generation of hadrons, which would generate critical fluctuations in the vicinity of the critical point of the phase transition.

Interestingly the higher statistical moments, the Kurtosis and Skewness still showed a non monotonic behavior (Figs. 6, 7, 8, 9). We presented these for the highest energy collisions, where the applicability of the applied EoS is the least questionable. These higher moments of specific energy densities show changing signs of the Kurtosis and Skewness.

Apart of the fact that the FD model provides a spatial distribution, Fig. 8 shows that the variation of higher moments is also sensitive to the FO time. This time can-

not be securely determined from within the FD model, and the final hadronization and freeze-out should be described by the last model stage of the hybrid model. Thus, we did not study the excitation function of the higher moments, because an arbitrary choice of the FO time may result in different results. On the other hand the time dependence of higher moments obtained here (Figs. 6-9) is different from the straightforward expectation arising from a dynamical phase transition [20].

The spatial fluctuations of specific energy and baryon charge density certainly influence the final baryon charge multiplicity and specific energy distributions. In the absence of other dynamical effects during hadronization the fluctuations of the fluid dynamical densities will be inherited by the corresponding final measurable quantities.

The present calculations show that in dynamical systems, even with the least initial variation, strongly varying higher statistical moments may develop. Thus the effects of the FD expansion and of the final hadronization and freeze out should be separated. This can be done in theoretical hybrid models by evaluating separately both effects, and in experiments by mixed event methods (e.g. ref. [29]) or more specific correlation measurements.

-
- [1] M. Stephanov, K. Rajagopal, E. Shuryak, *Phys. Rev. Lett.* **81**, 4816 (1998).
- [2] M. Stephanov, K. Rajagopal, E. Shuryak, *Phys. Rev. D* **60**, 114028 (1999).
- [3] M. A. Stephanov, *Phys. Rev. Lett.* **102**, 032301 (2009).
- [4] Y. Zhou, S.S. Shi, K. Xiao, K.J. Wu and F. Liu, *Phys. Rev. C* **82**, 014905 (2010).
- [5] C. Nonaka, S.A. Bass, *Phys. Rev. C* **75**, 014902 (2007).
- [6] C. Nonaka, M. Asakawa, S.A. Bass, *J. Phys. G* **35**, 104099 (2008).
- [7] C. Nonaka, M. Asakawa, S.A. Bass, B. Muller, *Nucl. Phys. A* **830**, 291c (2009).
- [8] H. Niemi, G.S. Denicol, P. Huovinen, E. Molnar and D.H. Rischke, arXiv: 1203.2452v1 [nucl-th].
- [9] L.P. Csernai, V.K. Magas, H. Stöcker and D.D. Strottman, *Phys. Rev. C* **84**, 024914 (2011).
- [10] P. K. Kovtun, D. T. Son and A. O. Starinets, *Phys. Rev. Lett.* **94**, 111601 (2005).
- [11] L.P. Csernai, J.I. Kapusta and L.D. McLerran, *Phys. Rev. Lett.* **97**, 152303 (2006).
- [12] T. Schafer and D. Teaney, *Rept. Prog. Phys.* **72**, 126001 (2009).
- [13] P. C. Hohenberg and B. I. Halperin, *Rev. Mod. Phys.* **49**, 435 (1977).
- [14] L.P. Csernai, D.D. Strottman and Cs. Anderlik, *Phys. Rev. C* **85**, 054901 (2012).
- [15] V.K. Magas, L.P. Csernai and D.D. Strottman, *Phys. Rev. C* **64** 014901 (2001).
- [16] V.K. Magas, L.P. Csernai and D.D. Strottman, *Nucl. Phys. A* **712**, 167 (2002).
- [17] Tapan K. Nayak for the STAR collaboration, *Nucl. Phys. A* **830**, 555c-558c (2009).
- [18] R.V. Gavai and S. Gupta, *Phys. Rev. D* **78**, 114503 (2008).
- [19] L. P. Csernai, Z. Neda, *Phys. Lett. B* **337**, 25 (1994).
- [20] L. P. Csernai, G. Mocanu and Z. Neda, *Phys. Rev. C* **85**, 068201 (2012).
- [21] L.P. Csernai and J.I. Kapusta, *Phys. Rev. Lett.* **69**, 737 (1992).
- [22] L.P. Csernai and J.I. Kapusta, *Phys. Rev. D* **46**, 1379 (1992).
- [23] P. Huovinen and P. Petreczky, *J. Phys. G*: **38**, 124103 (2011).
- [24] Ben-Hao Sa, Dai-Mei Zhou, Yu-Liang Yan, Xiao-Mei Li, Sheng-Qin Feng, Bao-Guo Dong and Xu Cai, *Comp. Phys. Commun.*, **183**, 333 (2012).
- [25] J. Cleymans, H. Oeschler, K. Redlich and S. Wheaton, *Phys. Rev. C* **73**, 034905 (2006).
- [26] N.S. Amelin, E.F. Staubo, L.P. Csernai, V.D. Toneev and K.K. Gudima, *Phys. Rev. C* **44**, 1541 (1991).
- [27] Sz. Horvat, V.K. Magas, D.D. Strottman and L.P. Csernai, *Phys. Lett. B* **692**, 277 (2010).
- [28] Yun Cheng, L.P. Csernai, V. K. Magas, B.R. Schlei and D. Strottman, *Phys. Rev. C* **81**, 064910 (2010).
- [29] Dai-Mei Zhou, Ayut Limphirat, Yu-liang Yan, Yun Cheng, Yu-peng Yan, Xu Cai, Laszlo P. Csernai, Ben-Hao Sa, *Phys. Rev. C* **85**, 064916 (2012).